inferred from magnetic lineation. Figure 1b shows a symmetric distribution of residual geoid with respect to the West Philippine Basin's remnant ridge crest. In its vicinity, a decrease of the geoid for the age increment of 10 Myr is 2 and 1 m, respectively, to the NNE and SSW directions. The slope is steeper for the former, but the data for both limbs agree with that exhibited by the active mid-oceanic ridges.

Corner flow model

The eastward tilt of the total geoid over the entire Philippine Sea and that of the residual geoid over the basins east of the Palau–Kyushu Ridge (Fig. 3a, b) seem to lack a correlation with the basin's lithospheric structure. They must have originated from some causes in the asthenosphere underneath or deeper. As one such cause, a corner flow looks most pertinent. Corner flow is a flow of visco-elastic material in the asthenosphere induced by the subducting oceanic lithosphere. Of the two flow systems induced along the sinking slab's upper and lower sides, that on the upper side (landward) is the more important in the present discussion. McKenzie[29] showed that the maximum stress heating of the viscous flow is localized in the vicinity of the island arc, directly beneath the marginal sea's lithosphere. This suggests that the thermal diapir, as a cause of marginal sea opening, is generated in the asthenosphere where the corner flow's viscous stress heating is a maximum. Thus, the corner flow model, an apparent alternative to the thermal diapir model, can actually be compatible with, as well as complementary to, it. Rheology of mantle material is, however, generally not well known. In McKenzie's calculation, the asthenosphere's viscous flow was assumed to be newtonian. It was recently shown[30] that the regional geoid depends strongly on the power of non-newtonian constitutive equation ($\dot{e} = \eta\sigma^n$; η = constant) which gives the strain rate ($\dot{e}$) as a function of

stress (σ). McAdoo's model calculation with a sinking slab's dip of 60° showed that the exponent (n) of the constituent equation must be >3 for the slope of geoid over the marginal sea basin to tilt towards the fore-arc. Apparently, simulations for a sinking slab with much steeper thrust angles are needed to compare the numerical result with the data obtained from the Philippine Sea. The slope of the total geoid ranging from 0.8 to 1.6 m per 100 km over the Philippine Sea basin should impose an effective constraint on the rheological property of the model. It is not clear whether the corner flow is restricted within the mobile asthenosphere or, as the depth of deep-focused earthquakes indicates, penetrating into the Earth's deep interior. If the corner flow's convective cell is shallow, the slope of the residual geoid will be more appropriate for the theory.

Conclusion

In addition to the bottom topography, marine geology, magnetic anomaly and heat flow, the geoid derived from satellite altimeter data has proved useful in studying the marginal sea's history. The idea of comparing the geoid of marginal sea basins with that of the oceanic floor, where the lithosphere is in a pre-subduction state and is undisturbed from the bending effect, is probably the most important. Data of bottom topography and heat flow processed in a similar fashion will serve to develop a systematic theory of marginal sea formation. This study will be extended to other marginal seas in the Western Pacific Ocean.

1. Karig, D. E. Bull geol. Soc. Am. 82, 323–344 (1971).
2. Rapp, R. H. J. geophys. Res. 84, 3784–3792 (1979).
3. Horai, K. J. geophys. Res (in the press).
4. Watts, A. B. & Daly S. F. A. Rev. Earth planet. Sci. 9, 415–448 (1981).
5. Lerch, F. J., Klosko, S. M., Laubscher, R. E. & Wagner, C. A. J. geophys. Res. 84, 3897–3916 (1979).
6. Kahn, M. S. Geophys. J.R. astr. Soc. 48, 197–209 (1977).
7. Watts, A. B., Bodine, J. H. & Bowin, C. O. A Geophysical Atlas of the East and Southeast Asian Seas: Free Air Gravity Field (Geological Society of America, MC-25, Boulder, 1978).
8. Watts, A. B. & Talwani, M. Geophys. J.R. astr. Soc. 36, 57–90 (1974).
9. Mrozowski, C. L., Lewis, S. D. & Hayes, D. E. Tectonophysics 82, 1–24 (1982).
10. Watts, A. B., Talwani, M. & Cochran, J. R. Geophys. Monogr. 19, 17–34 (1976).
11. Fisher, G. A. et al. Init. Rep. DSDP Leg 6, 293–387 (1971).
12. Karig, D. E. et al. Init. Rep. DSDP Leg 31, 25–350 (1975).
13. Klein, G. de V. et al. Init. Rep. DSDP Leg 58, 21–545 (1980).
14. Kroenke, L. et al. Init. Rep. DSDP Leg 59, 21–483 (1981).
15. Hussong, D. M. et al. Init. Rep. DSDP Leg 60, 101–249 (1982).
16. Watts, A. B. & Weissel, J. K. Earth planet. Sci. Lett. 25, 239–250 (1975).
17. Mrozowski, C. L. & Hayes, D. E. Earth planet. Sci. Lett. 46, 49–67 (1979).
18. Haxby, W. F. & Turcotte, D. L. J. geophys. Res. 83, 5473–5478 (1978).
19. McAdoo, D. C. J. geophys. Res. 86, 6073–6090 (1981).
20. Katsumata, M. & Sykes, L. R. J. geophys. Res. 74, 5923–5984 (1969).
21. Uyeda, A. & Kanamori, H. J. geophys. Res. 84, 1049–1061 (1979).
22. Packham, G. H. & Falvey, D. A. Tectonophysics 11, 79–109 (1971).
23. Karig, D. E. J. geophys. Res. 76, 2542–2561 (1971).
24. Sleep, N. & Toksoz, M. N. Nature 233, 548–550 (1971).
25. Scholz, C. H., Barazangi, M. & Sbar, M. L. Bull geol. Soc. Am. 82, 2979–2990 (1971).
26. Karig, D. E., Anderson, R. N. & Bibee, L. D. J. geophys. Res. 83, 1213–1226 (1978).
27. Karig, D. E. & Moore, G. F. Tectonophysics 27, 97–118 (1975).
28. Minster, J. B., Jordan, T. H., Molnar, P. & Heines, E. Geophys. J.R. astr. Soc. 36, 541–576 (1974).
29. McKenzie, D. P. Geophys. J.R. astr. Soc. 18, 1–32 (1969).
30. McAdoo, D. C. On the Compensation of Geoid Anomalies due to Subducting Slabs (Technical memorandum TM82157, Goddard Space Flight Center, Greenbelt, 1981).
31. Herman, B. M., Anderson, R. N. & Truchan, M. in Am. Ass. petrol. Geol. Mem. 29, 199–208 (1979).

A demonstration of ocean acoustic tomography

The Ocean Tomography Group: D. Behringer[*], T. Birdsall[†], M. Brown[‡], B. Cornuelle[§], R. Heinmiller[§], R. Knox[‡], K. Metzger[†], W. Munk[‡], J. Spiesberger[‡], R. Spindel[||], D. Webb[||], P. Worcester[‡] & C. Wunsch[§]

[*] Atlantic Oceanic and Meteorological Laboratory of NOAA, Miami, Florida 33149, USA
[†] Cooley Electronics Laboratory, University of Michigan, Ann Arbor, Michigan 48109, USA
[‡] Scripps Institution of Oceanography, IGPP, La Jolla, California 92093, USA
[§] Department of Earth and Planetary Sciences, Massachusetts Institute of Technology, Cambridge, Massachusetts 02139, USA
[||] Woods Hole Oceanographic Institution, Woods Hole, Massachusetts 02543, USA

Over the past decade oceanographers have become increasingly aware of an intense and compact ocean 'mesoscale' eddy structure (the ocean weather) that is superimposed on a generally sluggish large-scale circulation (the ocean climate). Traditional ship-based observing systems are not adequate for monitoring the ocean at mesoscale resolution. A 1981 experiment mapped the waters within a 300 × 300 km square south-west of Bermuda, using a peripheral array of moored midwater acoustic sources and receivers. The variable acoustic travel times between all source–receiver pairs were used to construct the three-dimensional (time-variable) eddy fields, using inverse theory. Preliminary results from inversions are consistent with the shipborne and airborne surveys.
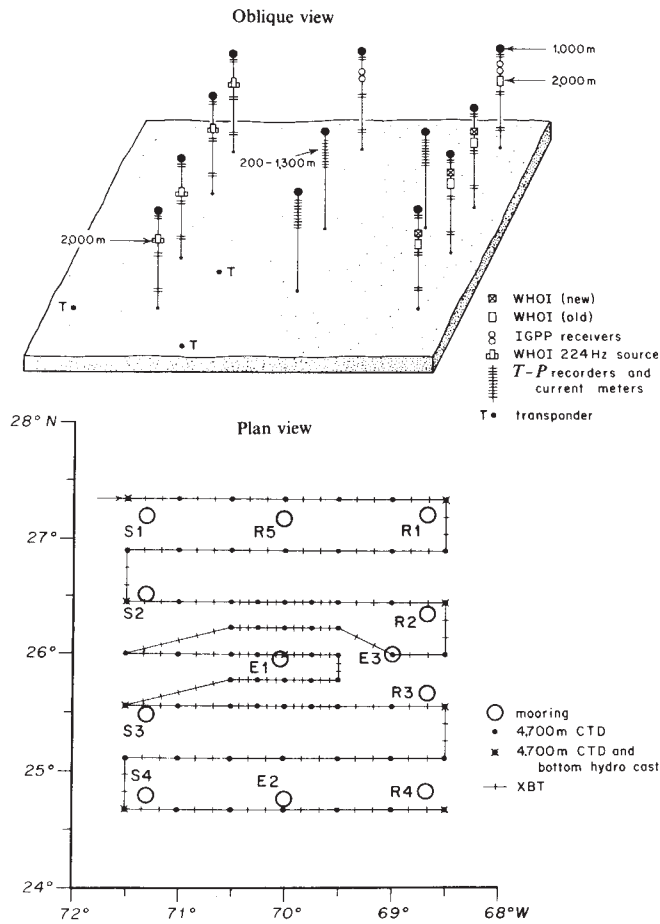
Oblique view

Plan view

Fig. 1 Geometry of the 1981 Ocean Tomography Experiment. S1 to S4 designate the acoustic source moorings, R1 to R5 the acoustic receiver moorings, and E1 and E2 the environmental moorings with current meters and temperature–pressure $(T-P)$ recorders. E3 is a current meter mooring set by F. Schott. Acoustic moorings also carried $T-P$ recorders. The receivers R1 and R5 consisted of short vertical arrays. Floats at 1,000 m depth with 1,000 lb buoyancy provided taut moorings, thus eliminating wave forces and reducing horizontal excursions. The position of each acoustic source and receiver was monitored by a 10-kHz source (placed just beneath the low-frequency tomographic sources and receivers) which interrogated three bottom transponders T dropped a few kilometres from the mooring (shown for S4). The plan view shows the grid for CTD/XBT surveys in March, May and July. In addition, AXBT drops at the CTD positions were carried out in April and June. The experimental area is over the Hatteras abyssal plain with depths varying between 5,300 and 5,600 m.

THE chief obstacle to understanding the ocean circulation is the overwhelming difficulty in observing it. The ocean is an enormous turbulent fluid fluctuating on all space and time scales. Largely as a result of the MODE expedition[1] in 1973, it has become clear that a 'mesoscale' variability, closely analogous to weather systems in the atmosphere, is superimposed on the large-scale ('climatic') flow field. But the mesoscales are disparate: a few months and several hundred kilometres in the oceans as compared with a few days and several thousand kilometres in the atmosphere.

There has been no perceived national or international requirement to lead towards a large-scale ocean observation network. The cost in ship time is prohibitive (10 full-time vessels for 1 Mm^2 (1,000 × 1,000 km, about one-third the Mediterranean). Interior *in situ* sensors cannot transmit data by conventional means because the ocean is opaque to electromagnetic radiation. For the same reason remote sensors in space cannot penetrate the ocean interior.

But the ocean is transparent to sound. Acoustic tracking of submarines goes back to World War I and tracking of neutrally buoyant floats from ships or shore stations is now a widely used oceanographic tool. However, there has been no previous

attempt to exploit the properties of the sound field itself as a way of attacking the fundamental observation problem.

The present experiment derives from a proposed scheme[2] for measuring the field of sound-speed fluctuations within a volume by acoustic transmission through the volume along many diverse paths. It was called 'ocean acoustic tomography', in analogy with the medical X-ray procedure CAT (for computer-assisted tomography). The procedure is best illustrated by reference to the 1981 experiment (Fig. 1). We chose a 300-km square in the same general area occupied by the MODE experiment[1] with a known mesoscale variability (MODE involved six ships and 25 conventional moorings). The 300-km dimension permitted adequate mapping from a ship in three weeks' time for comparison with the acoustic method, and the use of existing acoustic hardware. Sound pulses emitted at each of the four sources S were recorded at each of the five receivers R. Sound-speed in the ocean is predominantly a function of temperature; a cold eddy within the observation square will delay the arrival of any transmission through the eddy.

There is a minimum in sound-speed (Fig. 2) around 1 km depth forming a 'sound channel' which traps some of the acoustic energy. This waveguide, which is the dominant feature of mid-latitude acoustic propagation, is useful here in two ways: (1) acoustic rays that are refracted back towards the axis before intersecting the surface and bottom lose little energy through the boundaries and thus can be detected over several thousand kilometres (megametres), and (2) steep rays which sample the entire water column and generally arrive early can be distinguished from flat late rays which remain nearer the axis, and in this way something can be learned about the depth dependence of the ocean disturbances. A very shallow disturbance affects only the very steep rays with shallow upper turning points; a deep disturbance alters the travel times of both steep and shallow rays.

For each of the 20 source–receiver pairs (Fig. 2 represents one of these) we record roughly 10 multipaths, giving a total of about 200 travel times for each transmission. The number of data points grows geometrically with the product R × S, as compared with the sum R + S for conventional spot measurements and the path integration reduces the noise from local finestructure.

One needs a procedure for converting this information into maps or spectra (or other interesting representations) of the ocean temperature field. Generally the system is underdetermined, and there is an infinity of solutions. 'Inverse theory' can be used to constrain the solution by solving for the smoothest field, or finding the unique solution consistent with *a priori* knowledge of the field covariance. (The procedures of medical tomography are a specialized subset of the available mathematical tools.)

The procedure depends critically on the resolution, identification and stability of multipaths over large ranges. The scheme[2] proposed in 1979 depended on theoretical estimates, but there was no direct experimental evidence that any one of the three requirements could be met. Positive results, rather
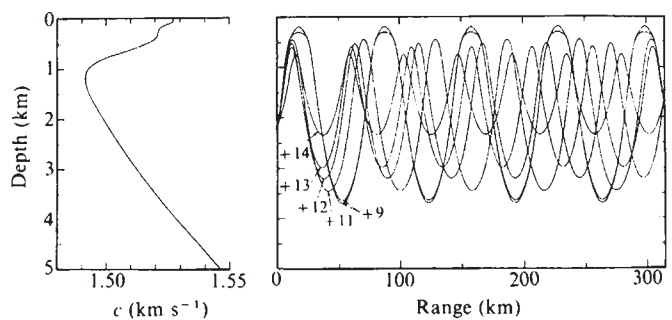

Fig. 2 Ray (multipath) diagram from source S1 to receiver R3 for upward (+) launch angles only. The identifier gives total (upper plus lower) number of ray turning points. The associated measured and predicted arrival structures are plotted in Fig. 3. The range-averaged sound-speed profile from S1 to R3 is shown to the left.
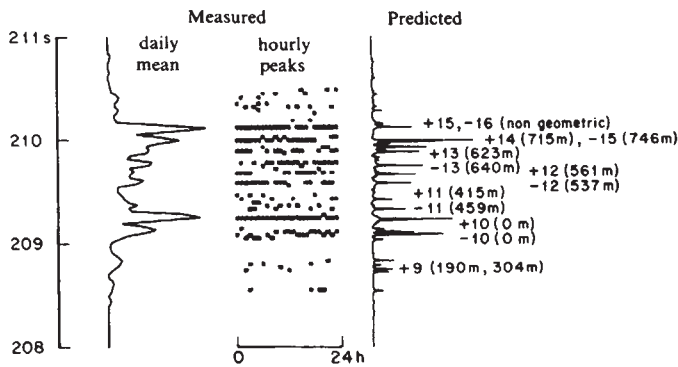
Fig. 3 Comparison of measured arrival pattern with the WKBJ predicted impulse response on year day 64 for S1 to R3 transmissions. The daily mean pattern is formed from 24 hourly transmissions. Travel times for the peak arrivals are shown for each hour. Only peaks with signal-to-noise ratios exceeding 15 dB are plotted. Selected arrivals are identified; for example, +14 (715 m) refers to an upward launch angle with 14 ray turning points, the upper turning point being at 715 m depth. Some of the associated rays are identified in Fig. 2. The non-geometric arrival refers to a ray with a turning point just above the receiver. Surface reflected a non-geometric arrivals are not included in Fig. 2.

better than expected, were subsequently obtained during 48 days of transmissions at 10-min intervals over a 900 km path eastwards from a source moored near Bermuda[3]. A northward 300-km transmission that was intersected by a southern meander of the Gulf Stream gave similar results[4]. These experiments also provided experience for solving two crucial engineering problems: mooring position keeping and time keeping.

Measurements

The acoustic sources are patterned after the neutrally buoyant SOFAR floats that have been used extensively to track subsurface circulation in the Atlantic[5,6]. Each source consists of four parallel 1-ft diameter aluminium tubes that are tuned for resonance at 224 Hz and have a bandwidth of 20 Hz. They are driven at the closed end by a flat circular plate of piezoelectric material. A microprocessor controls all source timing (on–off scheduling), including the phase modulation of its 224-Hz carrier. Briefly, the modulation is a 127-digit maximal length shift register sequence[7]. The autocorrelation function of the sequence is sharply peaked and has no sidelobes. Each digit comprises 14 cycles of the carrier and therefore has a duration of 62.5 ms. This is the width of the correlation peak and establishes the multipath resolution of the system. A sequence of 127 digits lasts nearly 8 s, which more than covers the time spread between the first and last arrivals (Fig. 3). A transmission consisting of 24 consecutive sequences lasts nearly 192 s, which is roughly the decorrelation time of the ocean due to internal waves for this experiment. Coherent averaging of the 24-sequence receptions affords signal-to-noise gain. One can think of each transmission as being equivalent to the transmission of 62.5 ms pulses at 8 s intervals repeated 24 times. Coherent summation produces a single intense pulse[8,9]. The transmitted power level is quite low, about 14 W (186 dB μPa^{-1} at 1 m), for a total of 2,700 J per transmission (about the same energy as in the prolonged grunt of a blue whale heard off the coast of Chile[10]) but when this energy is 'compressed' into 62.5 ms pulses it can be recorded at typically 25 dB signal-to-noise ratios, leading to a theoretical travel time precision of 2 ms for a resolved arrival.

The acoustic receivers are microprocessor controlled devices. The arrival time structure of the multipath field between source and receiver is obtained by cross-correlating the coherently averaged incoming signal with a stored replica of the transmitted signal. Some receivers performed the cross-correlation in situ and stored only the time of arrival of multipath peaks, while others simply stored signal samples for later on-shore processing. Reception times were synchronized to source transmission times. Transmissions were at hourly intervals (for tidal correc-

tion and to suppress internal wave noise) on every third day only (to conserve batteries).

To provide a time base accurate to better than 10 ms, each source and receiver was equipped with a rubidium atomic frequency standard to make daily measurements of the frequency offset of a considerably less stable (but of lower power) continuously running quartz crystal clock. The frequency offsets are integrated to yield time corrections. It is necessary also to correct the travel times for mooring excursions. These were measured with bottom transponders to a precision of ~1.5 m (1 ms for a line-of-sight displacement).

Travel times

The procedure depends critically on the resolution, identification and stability of multipaths over large ranges[3]. The predicted arrival pattern (Fig. 3) is derived from a generalization to ray theory[11], and it matches the measured pattern rather well. This identification, based on travel time, was checked for ray inclination at receivers R1 and R5 which were equipped with vertical arrays[12], and in no instance did the difference between measured and predicted inclination exceed the experimental error.

Figure 4 shows this arrival pattern on a reduced scale over a 100-day period. Multipath peaks are plotted as single points, and only those paths whose signal-to-noise ratio exceeded 15 dB are shown. The relative pattern is stable; some weak late arrivals are surface and bottom reflected and have not been used in the analysis. The 2 s drift of the raw pattern towards
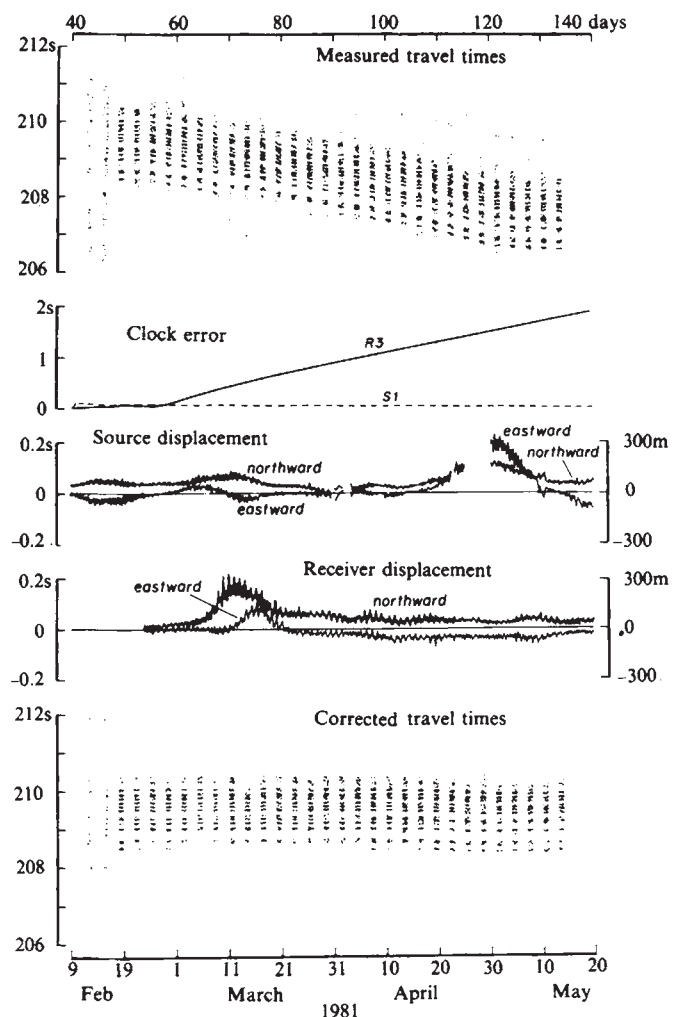

Fig. 4 Multipath arrival structure S1 to R3, before and after corrections for clock drifts and mooring displacements. Transmissions were over 24 h on each third day, starting 18 February (year day 49). The unstructured patterns on days 43 and 46 (before transmission) show processed noise. Gaps in the source displacement are due to missing data.

earlier arrival is almost entirely associated with the gain of the receiver clock (as measured by the rubidium standard). Horizontal excursions of the moorings provide a lesser correction. The high frequency excursions can be related to tidal motion. The arrival pattern corrected for clock drift and mooring motion provides the database for the tomographic inversion.

Comparison of tomographic with traditional measurements

There is a basic problem of comparing two fields that are not the same. The CTD (conductivity/temperature/depth) surveys took almost three weeks (during which time the fields changed); the acoustic surveys provided almost synchronous snapshots (one can think of them as surveys conducted at 3,000 knots).

Panels *b*, *e*, *f*, *i* of Fig. 5 show the sound-speed maps from the first two CTD/XBT cruises[13]. Nominal station spacing was 50 km but near the centre the spacing was halved (Fig. 1). During the second cruise 10 additional 1,500-m CTD casts extended the grid 100 km westward. Panel *a* was inferred (using representative *T–S* relations) from AXBT drops on 13–14 April at positions of the CTD stations. (The AXBT's were from P-3 aircraft supported by NAVOCEANO. Standard AN/SSQ36 probes (to 300 m depth) were used, with temperature calibrations (to ±0.15 °C) as described in ref. 14.) Sound-speed was computed[15] and then contoured using an objective interpolation scheme like that used in MODE[16]. The necessary weights were computed using a gaussian correlation function of 100-km scale.

The March map (days 66–85) shows a cold eddy nearly in the centre, evidently embedded in a background gradient with warmer water to the north. The May map (days 120–139) shows the same cold eddy displaced about 200 km to the west weakened, and perhaps split in two. A new cold eddy, smaller than the original, has appeared in the south-eastern corner.

The four central charts are from the tomographic inversion. The sound-speed field is modelled by specifying a covariance function for the perturbations around a basic state. The horizontal covariance function is homogeneous, isotropic and gaussian with a decay scale of 100 km. The vertical structure is made up of empirical orthogonal functions calculated from the MODE dataset[1].

The tomographic maps show a slow westward movement and slight weakening of the central cold eddy, and the appearance of a new cold centre in the south-east corner, consistent with the CTD surveys. A premature failure of receiver R4, followed by R2 and R3, has so far prevented the plotting of the tomographic chart for the time of CTD II, as had been intended. (The failures were the result of a faulty battery batch; the remaining receivers and all sources functioned normally and will eventually permit limited inversions through the full experimental period.) The chart sequence as shown implies a remarkably stable pattern for the first 40 days, followed by rapid changes in the subsequent 20 days. This interpretation of a 'jumpy' eddy movement is consistent with the observed stability in travel time to R1 until day 110, with rapid changes thereafter in the sense indicated by the charts in Fig. 5. Similarly, 'stick charts' of the measured currents at the environmental moorings E1 and E2 are uneventful until day 110 and then change rapidly[13]. The indicated sequence is as follows[13]:

● Days 62–91: A large cold eddy remains nearly stationary at a position north-east of E1 where it was observed during CTD I. Under its influence the E1 currents flow generally to the south-east and the E2 currents flow to the east.

● Days 91–110: The cold eddy moves slowly WSW to a position west of E1, near where it was seen during the AXBT flight on day 103. (This corresponds to the times of the tomographic inversions.) As a result the flow of the shallow E1 current meter (137 m) turns counterclockwise to the north, and the
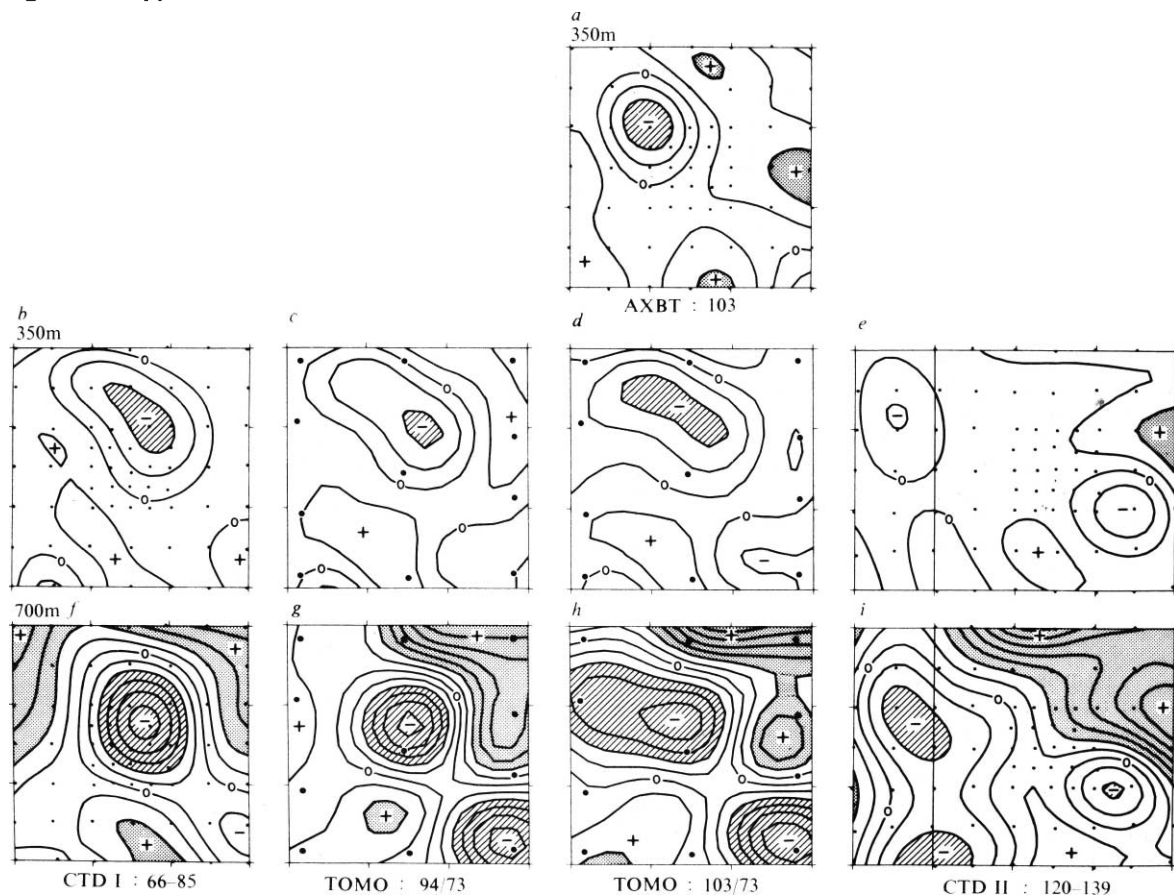

Fig. 5 Mosaic of sound-speed anomaly charts in the 300 × 300 km square (centred at 26° N, 70° W). *b, f* are from the first CTD survey, *e, i* from the second CTD survey (CTD II includes an additional 100 km strip to the west); *a* is from the AXBT survey. The four central charts are from the tomographic inversions, assuming travel time error bars of 10 ms. Year days 1981 are indicated below; the tomographic inversions are referenced to the travel time on day 73. *f–i* at 700 m depth gives sound-speed departures δ*C* relative to 1,505.9 m s⁻¹; *a–e* at 350 m depth relative to 1,521.7 m s⁻¹, with contour interval 1 m s⁻¹; departures above +2 m s⁻¹ and below −2 m s⁻¹ are shaded. Points give positions of CTD and AXBT casts, and of acoustic and environmental moorings (see Fig. 1 for mooring identification).
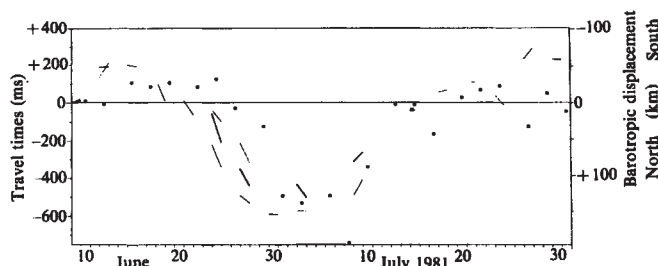
Fig. 6 Relative travel times at hourly intervals for every third day (transmission day) from two sources to north station are portrayed by the sloping line segments; short or missing lines are the result of low signal-to-noise levels. The right-hand scale shows the corresponding barotropic displacement of the Gulf Stream. •, Positions of the North wall of the Gulf Stream inferred from sea-surface temperature measured by NOAA-6 satellite.

flow of the deep (835 m) current meter turns completely around to the west. (The different degrees of turning of the shallow and deep current meters are caused by the north-east tilt of the eddy axis.) The flow of E2 turns slightly clockwise to the ESE.

● Days 110–130: The first cold eddy rapidly moves west to the edge of the experimental box and a second cold eddy appears in the south-east quadrant, where they are seen during CTD II. The flow is generally to the north-west at E1 and south-west at E2.

The above interpretation is supported by the good agreement between the measured currents and those from the dynamic height maps during CTD I and CTD II. We conclude that the tomographic inversions are consistent with the CTD and current meter observations.

The tomographic charts in Fig. 5 are the result of preliminary inversion for a few transmission days, using only a few paths per source–receiver pair. Work is in progress to optimize the procedure and to attempt inversions subsequent to day 103 with the degraded array (unfortunately the number of data points not only grows but also declines geometrically with the number of moorings).

There are two basic problems with the inversion process: initialization and linearization; work on these problems has started. In this preliminary report we follow the simplest initialization procedure: for each source–receiver pair we use only the difference in travel time reckoned from the (known) ocean state on day 73 to compute perturbation fields relative to day 73, and map the combined (initial plus perturbation) fields. For very long time series one would refer the perturbation maps to a climatological mean state which (probably) suffices for ray identification purposes. (Doubtful cases could be tied down with AXBT flights.) Any errors in the assumed mean state will, of course, be retained in the combined maps.

An equivalent (and better) procedure is to use absolute travel time for the known initial (or mean) ocean state to correct the array configuration for a navigational error of ±0.5 km, and to use absolute travel times in the subsequent inversions. (This involves only 15 independent constants, for example, the x, y positions of eight moorings relative to some arbitrary reference mooring, plus an arbitrary coordinate rotation. The present procedure involves 20 independent constants, for example, the absolute travel times on day 73 for each source–receiver pair.)

Formally, the tomographic procedure is independent of CTD surveys; these are used only to remove navigational errors. It

is expected that the GPS satellite system and sea floor localization procedures[17] will determine the configuration of future arrays to within ±1 m. At this point a knowledge of the climatological state is required only for ray identification, and the perturbation maps are free from initialization error.

In our linearized inversion procedure we ascribe perturbations in travel time to perturbations in sound-speed along the unperturbed ray paths. But rays emerging from mesoscale eddies have turning depths that may differ sufficiently from the unperturbed turning depths so that a significant part of the travel time perturbation is accumulated outside the eddy[18]. Generally the errors are too large to be neglected, yet sufficiently small to suggest an iteration procedure[19]. This has not yet been attempted.

Remote stations

The sources were monitored at remote facilities to assure their proper functioning, and to gain experience with long-range transmissions. In this connection we observed a systematic fluctuation in travel time over a northward 2,000-km path across the Gulf Stream (Fig. 6). (On calendar days 52, 55, 58 the receptions from source S2 were poor; on day 61 this source was recovered, found faulty, and another source deployed. No other source anomalies were seen during the remaining six months.) At the midpoint of the 50 days record, the travel time was shortened by 0.8 s. This is the result of a 200-km northward displacement of the Gulf Stream, with the associated decrease in the amount of cold slope water over the path[20]. (Satellite sea surface temperatures support this interpretation.)

Discussion

The preliminary report of the 1981 experiment indicates that ocean mapping with mesoscale resolution can be performed tomographically over substantial areas. There is, of course, a shortcoming in measuring only the sound-speed field. But in regions of tight T–S relations, or where the disturbances are associated mostly with vertical displacements of the isopycnals, the sound-speed perturbation can be mapped into density perturbations with accuracies adequate for computing geostrophic currents[21].

Two developments are planned for the future. In the autumn of 1982 we plan to make reciprocal transmissions[22] at 300 km ranges and use the difference in the oppositely directed travel times to infer the water velocity along the ray paths (velocity tomography). Subsequently we plan to establish an array of megametre dimensions to measure the variability of an ocean gyre[23]. Here the tomographic principle would be used to obtain vertical resolution; in the horizontal directions advantage is taken of the integrating properties of long range sound transmissions, opening the way to true ocean-basin scale measurement programmes.

1. The MODE Group *Deep-Sea Res.* **25**, 859 (1978).
2. Munk, W. & Wunsch, C. *Deep-Sea Res.* **26A**, 123 (1979).
3. Spiesberger, J. L., Spindel, R. C. & Metzger, K. *J. acoust. Soc. Am.* **67**, 2011 (1980).
4. Spindel, R. C. & Spiesberger, J. L. *J. acoust. Soc. Am.* **69**, 982 (1981).
5. Webb, D. C. *Proc. Oceans '77 Conf. Rec. MTS-IEEE* **2**, 44B (1977).
6. Spindel, R. C., Porter, R. P. & Webb, D. C. *IEEE J. Oceanic Engng* **OE-2**, 331 (1977).
7. Golomb, S. W. *Shift Register Sequences* (Holden-Day, San Francisco, 1967).
8. Spindel, R. C. *Proc. IEEE Electron. Aerospace Convent.* **80 CH**, 1587-4AES, 165 (1980).
9. Spindel, R. C. *IEEE Trans. Acoustics, Speech Signal Processing* **ASSP-27**, 723 (1979).
10. Cummings, W. C. & Thompson, P. O. *J. acoust. Soc. Am.* **50**, 1198 (1971).
11. Brown, M. G. *J. acoust. Soc. Am.* (in the press).
12. Worcester, P. F. *J. acoust. Soc. Am.* **70**, 1743 (1981).
13. Behringer, D. W., Heinmiller, R., Knox, R. & Thomas, G. *NOAA Technical Rep.* (1982).
14. Sessions, M. H. & Barnett, T. P. in *Near Surface Ocean Experimental Technology Workshop Proc.* NORDA, 125 (1980).
15. Chen, C. T. & Millero, F. J. *J. acoust. Soc. Am.* **62**, 1129 (1977).
16. Bretherton, F. P., Davis, R. E. & Fandry, C. B. *Deep-Sea Res.* **23**, 559 (1976).
17. Spiess, N. F. (Chairman), *Panel on Ocean Bottom Positioning of the Committee of Geodesy* (National Academy of Sciences, Washington, DC, 1982).
18. Mercer, J. A. & Booker, J. R. *J. geophys. Res.* (submitted).
19. Spiesberger, J. L. & Worcester, P. J. *J. acoust. Soc. Am.* (submitted).
20. Spiesberger, J. L. *et al. J. phys. Oceanogr.* (submitted).
21. Worcester, P. F. & Cornuelle, B. *Proc. 2nd Working Conf. on Current Measurements* (in the press).
22. Worcester, P. *J. acoust. Soc. Am.* **62**, 895 (1977).
23. Munk, W. & Wunsch, C. *Phil. Trans. R. Soc.* (in the press).